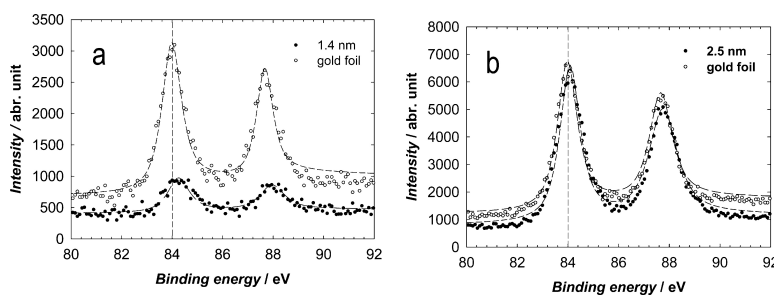


Combinatorial Approach to the Study of Particle Size Effects in Electrocatalysis: Synthesis of Supported Gold Nanoparticles

Samuel Guerin, Brian E. Hayden, Derek Pletcher, Michael E. Rendall, Jens-Peter Suchsland, and Laura J. Williams

J. Comb. Chem., **2006**, 8 (5), 791-798 • DOI: 10.1021/cc060040k • Publication Date (Web): 22 July 2006

Downloaded from <http://pubs.acs.org> on March 22, 2009



More About This Article

Additional resources and features associated with this article are available within the HTML version:

- Supporting Information
- Links to the 3 articles that cite this article, as of the time of this article download
- Access to high resolution figures
- Links to articles and content related to this article
- Copyright permission to reproduce figures and/or text from this article

[View the Full Text HTML](#)

Combinatorial Approach to the Study of Particle Size Effects in Electrocatalysis: Synthesis of Supported Gold Nanoparticles

Samuel Guerin, Brian E. Hayden,* Derek Pletcher, Michael E. Rendall, Jens-Peter Suchsland, and Laura J. Williams

School of Chemistry, University of Southampton, Southampton SO17 1BJ, UK

Received April 3, 2006

A high-throughput method for physical vapor deposition has been applied to the synthesis of libraries of supported gold particles on amorphous substoichiometric TiO_x and carbon supports. The TiO_x substrate stoichiometry can be varied or kept constant across a supporting sample, and subsequent deposition of particle sizes on supports are controlled through the nucleation and growth process. TEM measurements indicate nucleation and growth of Au particles takes place, with the smallest particles initially observed at 1.4 nm with a maximum density of $5.5 \times 10^{12} \text{ cm}^{-2}$ on titania, and 2.6 nm with concomitantly lower density on carbon. The 1.4-nm particles on titania exhibit a binding energy shift in the Au(4f) core level of 0.3 eV from bulk gold, and the shift is ~ 0.1 eV by the time particles grow to a mean size of 2.5 nm. These shifts are associated with final state effects, and the supported gold particles are metallic and appear to be relatively stable in air. When combined with appropriate substrates and screening techniques, this method provides a highly controllable method for the high-throughput synthesis of model supported catalyst.

Introduction

Guerin and Hayden¹ have recently described a physical vapor deposition system that employs source shutters to achieve a controlled gradient of deposited elements across a substrate or an array of pads appropriate for combinatorial screening of new materials. When combined with instrumentation that allows the simultaneous measurement of voltammetric responses at an array of electrodes,² one has a powerful high-throughput approach to the optimization and understanding of electrocatalysts. For example, the method has been applied to the optimization of Pd/Pt/Au continuous thin film electrocatalysts.³ This paper describes the application of the high-throughput physical vapor deposition (HT-PVD) method¹ to the fabrication and characterization of arrays of electrodes designed to address the optimization and understanding of other parameters in electrocatalysis and, indeed, heterogeneous catalysis in general; namely, the selection of support and the size of supported particles. Both the size of supported metal particles and the support itself can strongly influence the activity, selectivity, and stability of these catalytic systems.

Carbon is the most common support for electrocatalysts in fuel cells, but it is known to undergo some corrosion in operating conditions, particularly at the oxygen cathode.^{4,5} Moreover, it is widely recognized that the substrate can have a strong influence on the performance of a dispersed metal catalyst. As a consequence, there is considerable interest in the study of alternative substrates for electrocatalysis. The substrate must be sufficiently conductive and be stable in the environment found in the fuel cell. Oxides, particularly the so-called dimensionally stable anodes based on RuO_2

and IrO_2 , have enjoyed much success in electrochemical technology.⁶ Oxides, therefore, offer both potential for stability and conductivity and are also known to influence the activity of supported metal particles.

Titania is stable in acid environments (such as those found in polymer electrolyte membrane (PEM) fuel cells), is available in high surface area forms, and can be rendered sufficiently conducting to act as a support by its use in substoichiometric or doped forms. Hence, it was selected as a substrate to compare with carbon. Gold was selected as the catalyst material. Highly dispersed Au centers on metal oxide supports, including titania, have engendered considerable excitement because they exhibit unusual and unexpected catalytic activity for a number of gas-phase oxidations,^{7–9} and some possibilities for applications in fuel cell technology have been outlined.¹⁰ The enhanced catalytic activity of the gold centers on oxide substrates is found when the particles have a diameter in the range of 1–4 nm, but the reasons remain unclear, and a number of theories have been advanced.^{11–19}

Experimental Section

The deposition of both substrate layers and gold nanoparticles was carried out in a multichamber, ultrahigh-vacuum (UHV), molecular beam epitaxy system modified for high-throughput synthesis of graded compositions of thin film materials.¹ The growth chamber employed here incorporated three Knudsen cell (K-cell) sources (DCA HTKS) and an electron gun (e-gun) evaporation source (Temescal). The operational base pressure of the system is $< 5 \times 10^{-10}$ mBar rising to 1×10^{-9} mBar during metal deposition. Titanium layers, titania layers, and gold particles were deposited from titanium granules (99.95%, Goodfellow Metals) and gold

* To whom correspondence should be addressed. E-mail: beh@soton.ac.uk.

pellets (99.99%, Goodfellow Metals) in K-cells. Substoichiometric TiO_x layers (typical thickness 65–85 nm) were deposited by the oxidation of the titanium during deposition by a beam of molecular oxygen (BOC Special Gases, N6 Grade) at a pressure of 1×10^{-7} mBar directed at the sample face. For particularly stoichiometric titania films, a 600-W RF atom plasma source (MATS30, Mantis Deposition) was used to generate atomic oxygen that was directed at the sample by a highly polished quartz collimator. Carbon layers (typical thickness 30–60 nm) were deposited using the e-gun evaporation source and graphite rods (Alfa Aesar, type 231-955-3). Carbon layers were also deposited (where indicated) by means of an arc carbon-coating system (BOC Edwards) using carbon rods (BOC Edwards, type E085-19-030). In both cases, the uniformity was excellent, and the conductivity of the carbon layer was found to be $3 \times 10^2 \text{ S cm}^{-1}$, similar to the value reported for evaporated amorphous carbon of $\sim 10^3 \text{ S cm}^{-1}$ found in the literature.²⁰ The thicknesses of the C or TiO_x deposit were controlled by the deposition time, and sample thickness was established by calibration of growth rates from AFM measurements.

AFM (Veeco, Autoprobe M5) was carried out in tapping mode using a silicon cantilever with a resonance frequency of $\sim 180 \text{ kHz}$, spring constant of 5 N m^{-1} and tip curvature radius of $\sim 1 \text{ nm}$ (μ -mash; DP14/HIRES/AIBS) or in noncontact and contact mode (ThermoMicroscope Ultralever UL06A and UL20A) for particle height determination. Ellipsometry (Nanofilm i-elli2000) at 532 nm was used to confirm the thickness and gradation of deposits across the wafers. The ellipsometer was adapted to operate in a rotating compensator mode. The values of the angles Δ and ψ have been obtained by Fourier transformation of the intensities vs the azimuth of the compensator.²¹ Measurements were taken under a constant incident angle of 60° , and a computer-controlled macro enabled an automated mapping of 100 points over the substrate. Uniformity of deposition was demonstrated by four-point probe resistivity measurements at multiple points over the surface using a Four Dimensions 280DI automated conductivity mapping system. A four-point probe head (Jandel, A-type, $< 60 \text{ g}$ tip pressure) with 1-mm spacing or a square array head (1-mm spacing, Jandel) were used to measure the film sheet resistances. The probe heads were cleaned repeatedly by contact to a ceramic cleaning sheet to ensure reproducibility between films.

The gold particles were deposited by PVD with a source temperature, T_{dep} , of 1548 or 1623 K, yielding a highly stable Au flux equivalent to the deposition of $0.16 \pm 0.015 \text{ nm min}^{-1}$ and $0.51 \pm 0.05 \text{ nm min}^{-1}$. Deposition rates were calculated by the deposition of several thick layers over extended times and demonstrating that the thickness (as determined on contact masked samples by AFM) was proportional to the deposition time. The particle sizes across the arrays were subsequently controlled over concomitantly shorter times through the shutter position, the deposition time, and substrate temperature (298–308 K). Due to the macroscopic size of the PVD source and the positioning of the shutter, a “wedge” distribution of material over the sample is accomplished.¹ The particle size distribution and number of particles per square centimeter as a function of deposition

time were determined by transmission electron microscopy (TEM) by deposition of the gold onto small carbon-coated copper TEM grids (Agar, 400 grid) that had been additionally coated with a thin layer (20–60 nm) of either C or TiO_x ; conditions for deposition of both substrate and gold were identical to those used for coating the arrays and disks. TEM images were obtained using a JEOL 3010 with an accelerating voltage of 300 kV incorporating a Gatan CCD camera for recording images. XPS measurements were carried out in a UHV system incorporating a twin anode X-ray source (Al $K\alpha$ and Mg $K\alpha$) and a VSW clam single channel XPS analyzer.

Depositions were carried out onto (a) silicon, (b) silicon nitride (65 nm) on silicon, (c) a microfabricated silicon (10×10) array of gold electrodes for electrochemical measurements,³ and (d) Ti disks. Before deposition, the Ti disks were polished with $6\text{-}\mu\text{m}$ down to $0.1\text{-}\mu\text{m}$ diamond suspension (Kemet International) on a Microcloth (Buehler) and subsequently etched in a solution of 80 parts water, 18 parts HNO_3 (Fisher Scientific; Laboratory Reagent grade), and 2 parts sodium fluoride (BDH Chemicals; General Purpose Reagent grade) at room temperature for 20 min. The titanium disks (5-mm diameter) were mounted in a holder that allowed 16 disks to be coated simultaneously in the PVD system. The disks were first coated with Ti (2–5 nm) to improve adhesion of the layer of TiO_x . In the case of the (10×10) arrays, it was found that TiO_x did not adhere well to the gold electrodes. Prior to deposition of the TiO_x , a 12-nm layer with a composition close to Ti metal was deposited using the lowest possible oxygen pressure, before the oxygen pressure was increased to synthesize TiO_x , providing good adhesion to the electrode. The PVD system could be set up to give a uniform flux of Au over the Ti disks (constant particle size) or a “wedge” deposition to mimic the variable particle distributions on the arrays.

Results and Discussion

Deposition of Uniform TiO_x Layers. TiO_x layers were initially deposited onto silicon nitride-coated silicon using the Ti (K-cell) and molecular oxygen (10^{-10} – 10^{-5} mBar) directed at the substrate using a collimating source positioned to one side of the sample. The substrate temperature was typically 298–323 K. Subsequent AFM measurements established growth rates of $\sim 2.2 \text{ nm min}^{-1}$, and film thicknesses were typically in the range 50–100 nm. Effective variation of stoichiometry was qualitatively indicated by the change in color^{22,23} of the synthesized film with oxygen pressure: TiO_x deposited with an oxygen pressure of 10^{-7} and 10^{-9} mBar produced blue and brown films respectively, and XRD indicated that the titania films were largely amorphous.

Since the conductivity of titania is a strong function of stoichiometry,²⁴ and for applications of titania as a support for electrocatalysis, conductivity is a requirement, the sheet resistances of the films were measured (mapped) as a function of position over the thin film sample using the four-point probe method. Figure 1a shows a resistance map for a 66-nm-thick TiO_x film prepared with an oxygen pressure of

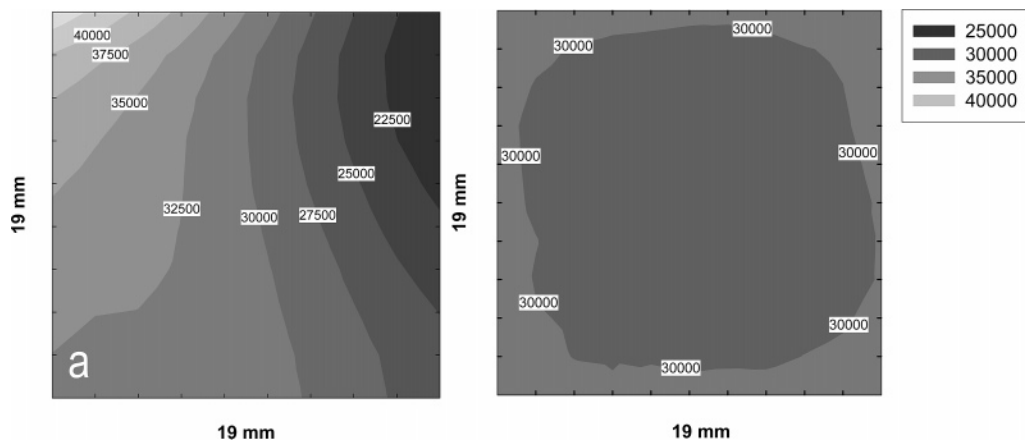


Figure 1. Sheet resistance (Ohms per square) contour plots of 100 measurement points on titania thin films. Samples prepared at a partial pressure of molecular oxygen of 1×10^{-7} mBar at a Ti K-cell temperature of 2073 K over 1800 s. (a) Anisotropic oxygen flow, (b) sample rotated during deposition.

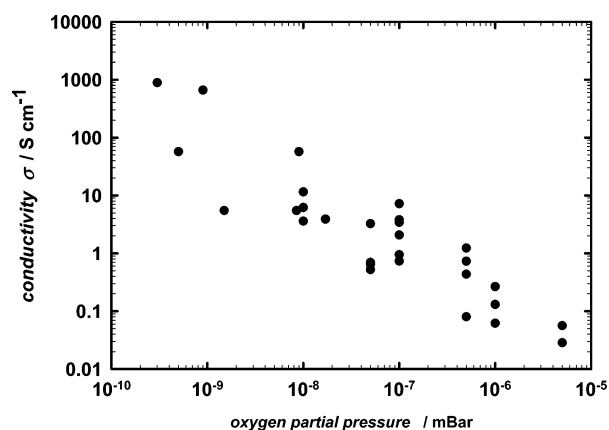


Figure 2. Experimentally determined conductivities (calculated from film thickness and measured sheet resistance) of various substoichiometric titania films prepared at different partial pressures of oxygen.

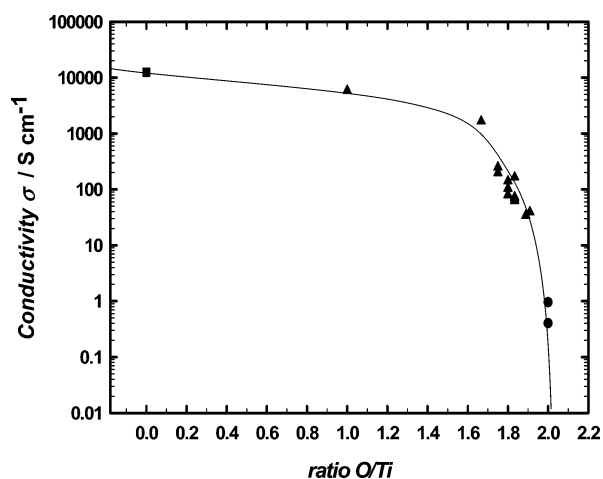


Figure 3. Comparison of titania conductivities from the literature vs the ratio of oxygen over titanium. Data taken from ■, ref 26; ▲, ref 25; and ●, ref 24.

10^{-7} mBar. There is a variation in the sheet resistance across the sample associated with a variation in stoichiometry due to the anisotropic exposure to oxygen of the titania during growth. This observation provides evidence that if optimized, collimated molecular oxygen beams may be used to synthesize graded stoichiometries of oxides for high-throughput thin

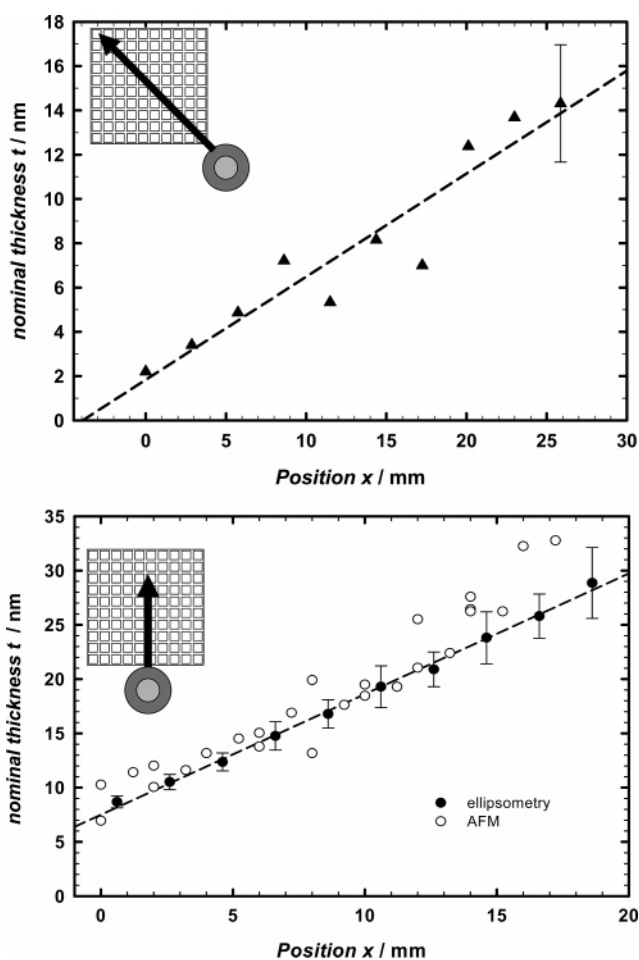


Figure 4. Thickness determination of gold deposition onto a bare silicon wafer using a 10×10 contact mask in two geometries (see inset) using (a) AFM along the diagonal of an array of 100 fields, and (b) using AFM and ellipsometry for a deposition geometry that allowed an averaging of 10 fields of identical thickness across the “wedge”(see insets). The source temperatures and deposition times were (a) 1548 K, 7200 s and (b) 1623 K and 4500 s.

film synthesis. Alternatively, and for the subsequent measurements carried out in this study, this variation is removed by rotating the sample during the deposition process: Figure 1b shows homogeneous stoichiometry of titania when synthesized in this way, with constant sheet resistivity observed across the sample. The small deviations in resistiv-

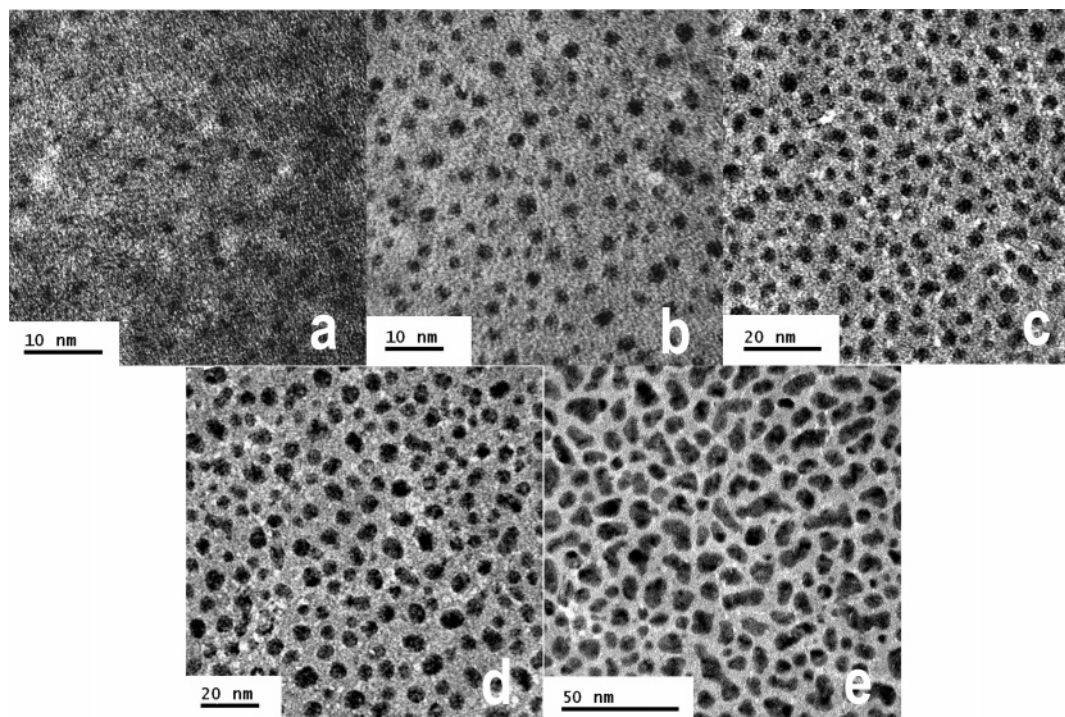


Figure 5. TEM micrographs of titania-supported gold particles. The nominal thickness of gold was (a) 0.13, (b) 0.78, (c) 1.56, (d) 2.33, and (e) 3.16 nm, and the deposition rate was $2.6 \times 10^{-3} \text{ nm s}^{-1}$.

ity at the sample edges is primarily a result of the four-point probe measurement resulting from anisotropic current distributions.

Figure 2 shows the variation of the conductivity of the TiO_x film (calculated from the sheet resistances and the film thicknesses determined by AFM) as a function of the synthesis oxygen pressure. The conductivity varies over more than 4 orders of magnitude over the pressures of molecular oxygen used for synthesis and may be associated with oxygen deficiencies within the rutile structure²⁴ that increase as the oxygen pressure is lowered during deposition. To estimate the stoichiometry of the TiO_x , the results were compared (Figure 3) to materials for which both stoichiometry and conductivity are known.^{24–26} For example, a significant amount of data is available because of the interest in the Magneli phases of titanium oxides, particularly Ti_4O_7 and Ti_5O_9 , as corrosion-resistant materials with conductivities high enough to be considered as electrodes in massive form. We conclude that the titania thin film synthesis carried out in this study using molecular oxygen produced stoichiometries in the range $x \sim 1.7–1.9999$. We have also been able to synthesize near-stoichiometric titania thin films using a plasma atom source, with concomitantly much higher resistivity. For the titania-supported gold samples, the titania was synthesized using 1×10^{-7} mBar of molecular oxygen, corresponding to a conductivity of $\sim 3 \text{ S cm}^{-1}$ and a stoichiometry of $x \sim 1.96$, estimated from comparison with materials produced elsewhere (Figure 3).

Amorphous carbon layers (carbon coating system) have been deposited, and the uniformity and resistivity of the films was investigated by four-point probe measurements. The films exhibited a conductivity of $\sim 3 \times 10^2 \text{ S cm}^{-1}$, and the variation across the substrate was found to be 0.5%. This

deviation was found at the edges of samples and ascribed to the edge effecting the four-point probe measurement.

Deposition of Gold Nanoparticles on Uniform TiO_x Layers. Gold was deposited using the K-cell at 1548 and 1623 K, producing a highly stable Au flux and deposition rate of 0.16 or 0.51 nm min^{-1} . Variable coverages over the substrate were deposited under the same conditions using the fixed “wedge” shutter.¹ The characteristic of the “wedge” growth was established (Figure 4) from AFM and ellipsometry measurements of gold deposited for times sufficient to achieve continuous films, and concomitantly lower times were used subsequently to achieve the lower nominal coverages required for particle growth. Two examples are shown in Figure 4, with different orientations of the source with respect to the substrate and different shutter positions. In Figure 4a, a uniform nominal thickness of $\sim 18 \text{ nm}$ would be achieved in the absence of the wedge shutter. AFM measurements show a variation of a factor of 7 in coverage is achieved across the (10×10) array. It was the relatively large error associated with the AFM results that resulted in additional ellipsometric determination of film thickness. In Figure 4b, gold was deposited using a geometry (inset) which produced 10 rows of fields of different thicknesses, each row consisting of 10 fields with the same thickness (deposition perpendicular to the “wedge” direction is constant¹). In this case, the wedge was characterized by less variation of thickness (8.9–28.9 nm). The thickness determined from ellipsometry has been estimated assuming for gold ($\tilde{n} = 4.1502 - 0.0449i$) and for the silicon substrate ($\tilde{n} = 0.4666 - 2.4083i$). The native oxide layer on the Si before deposition has been ignored. The results are consistent with the AFM measurements and indicate a smooth and linear change in film thickness in the direction of “wedge” growth.

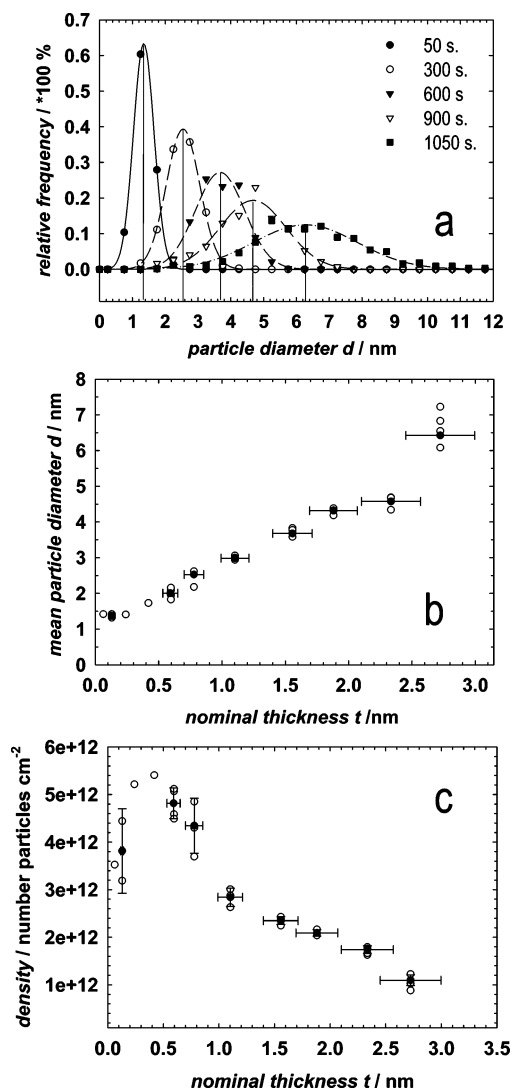


Figure 6. (a) Particle size distributions of gold particles grown on TiO_x obtained from TEM measurements. Gold deposition times are shown in the Figure. The data were fitted to a normal Gaussian function. (b) The mean particle size of gold. (c) The number of particles per square centimeter of particles per square centimeter.

For electrochemical studies,²⁷ gold particles were deposited onto TiO_x and carbon on both arrays and Ti disks using the conditions described above but with proportionally reduced deposition times to achieve low coverages and particle growth. Particle size distributions were measured by TEM. Both titania and carbon (~ 20 – 60 nm thickness), and subsequently the gold, were deposited on TEM microscope grids under conditions identical to those used for other substrates. Figure 5 shows TEM images for five deposition times (50, 300, 600, 900, and 1200 s) corresponding to nominal thicknesses of 0.13, 0.8, 1.6, 2.3, and 3.2 nm, respectively, of Au on TiO_x . The light field image clearly allows the identification of the gold particles that are near spherical in shape, distributed randomly at low coverages, and coalesce at higher coverages.

Figure 6 provides a quantitative analysis of the particle growth. From the particle size distributions in Figure 6a, it is evident that mean particle diameters are ~ 1.4 nm and fall in a narrow range of sizes at low at low nominal Au thicknesses, with both size becoming larger and distributions

Table 1. Summary of AFM Characterization of Titania and Titania-Supported Au Surfaces

nom. thickness of gold, t / nm	image size, nm^2	no. of particles incorporated	RMS ^a roughness / nm	TEM particle, d / nm	AFM height, H / nm	ratio TEM/AFM
0	500		0.78			
0	100		0.67			—
0.78	100	34	0.75	2.53	1.29	1.96
1.56	500	75	1.31	3.68	2.17	1.70
2.33	500	62	1.14	4.58	2.17	2.11

^a RMS roughness is defined as the square root of the mean value of the squares of the distance of the points from the image mean value: $\text{Rms} = \sqrt{(1/N) \sum_{i=1}^N \langle Z_i - Z \rangle^2}$.

becoming broader as the nominal thickness of Au increases. The change in mean particle size as a function of nominal thickness is shown in Figure 6b, and the number of particles per square centimeter is shown in Figure 6c. Initial stages of growth are characterized by an increase in the number of particles at near constant particle size (1.4 nm). This is followed by an increase in particle size and a reduction in the number of particles per square centimeter. This initial growth stage is associated with Au particle nucleation at titania defect sites, which may be surface oxygen vacancies that appear to stabilize clusters.²⁸ The ability to identify particles down to 1.4 nm in ex situ measurements and the stability of these particles to longer-term exposure to atmosphere (over 6 months) indicate that on the amorphous surface, there is little tendency to migration and agglomeration of particles at room temperature. Agglomeration has been observed on polycrystalline titania supports,²⁹ and we can only speculate that this difference may be due to the absence of grain boundaries or an increased defect density on our substrates and the concomitant stabilization of small particles. The growth mode observed here is similar to that observed using in situ low energy ion scattering (LEIS) measurements for $\text{TiO}_2(110)$ -supported Au particles³⁰ and subsequently ex situ high-resolution SEM,³¹ with the main difference being that the number of nucleation sites is larger and the observed particle sizes are smaller on the amorphous titania substrates. The latter may simply be associated with the higher defect density on the amorphous titania, and interestingly, they also report that the particles are stable in air.³¹

TEM did not allow an estimate of the shape or height of the Au particles. Although AFM was not able to provide sufficient lateral resolution to confirm particle sizes as a result of tip broadening, we attempted to establish particle height from the AFM measurements. Table 1 summarizes roughness factors and estimates of Au particle numbers and heights from a number of AFM images. Results are included for the root-mean-square roughness of the titania substrate and for several nominal thicknesses of gold. The root-mean-square roughness increases with increasing gold coverage. For gold particle height analysis, line measurements were taken at arbitrary positions of the image, and it was assumed that all features in this measurement were associated with the Au particles. Clearly, this is an approximation, since the titania also exhibits a finite, albeit lower, roughness. Comparing the ratio of the particle diameter from TEM versus

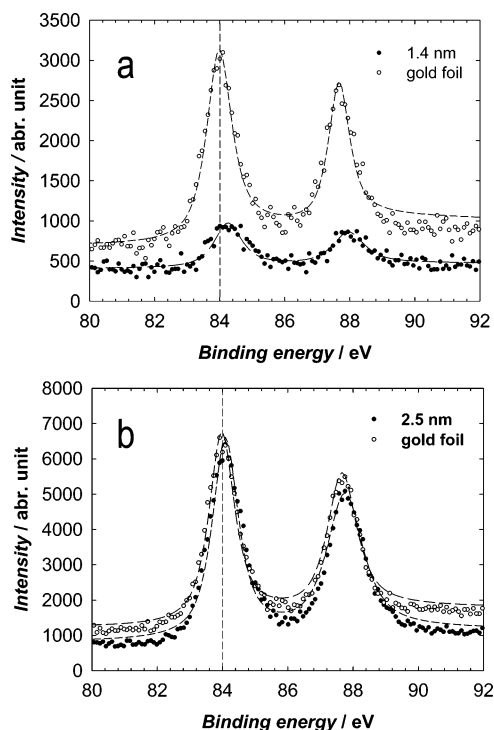


Figure 7. XPS spectra of the Au(4f) core level for titania-supported particles with a mean diameter of (a) 1.4 and (b) 2.5 nm. The calibration spectrum from a gold foil is also shown.

the “height” of the particle as measured by AFM, we consistently find values close to 2.

We conclude that the observed Au particles are hemispherical, which is consistent with previous conclusions on $\text{TiO}_2(110)$.³¹ Combining the number densities and particle sizes measured in TEM (Figure 6) of hemispherical particles allows an estimate of the Au surface area. This value is important, for example, in establishing specific electrocata-

lytic activity in reactions investigated on these model catalysts.

Figure 7a and b shows XPS spectra (Au(4f)) of titania-supported Au particles of 1.4- and 2.5-nm mean diameter. The peak positions of a gold foil, measured under the same conditions as the particles, has been included and provides a calibration reference for the Au 4f_{7/2} peak of bulk Au at 84.0 eV.³² A shift in the peaks for the 1.4-nm particles of ~ 0.3 eV to higher binding energy is observed, and this shift decreases to ~ 0.1 eV for 2.5-nm particles. The upward shift in binding energy for the small particle is similar to that found for Au on $\text{TiO}_2(110)$ during the initial growth stages and was associated with final state effects (electron screening in a small cluster) rather than any initial state effect.^{30,33} The shift is also similar to that found for 2-nm particles on polycrystalline titania,²⁹ where it was concluded that in addition to a final state contribution, an initial state effect also contributed to the shift from the bulk value.

Deposition of Gold Nanoparticles on Uniform Carbon Layers. Gold was deposited using the conditions described in the Experimental Section at a deposition rate of 0.16 nm min^{-1} onto carbon-coated TEM grids on which a 30-nm carbon film (carbon-coating system) was deposited to ensure the same substrate and nucleation behavior. Figure 8 shows the TEM images for gold particles on carbon with deposition times of 50, 300, 600, and 900 s (nominal thicknesses 0.13, 0.8, 1.6, and 2.3 nm, respectively). These images were analyzed to give the particle size distributions shown in Figure 9a; Figure 9b reports the variations of the mean particle diameter, and Figure 9c, the number of particles per square centimeter as a function of the nominal thickness. Comparison of these data with those in Figures 5 and 6 for the deposition of gold particles on TiO_x indicates a number of differences on the carbon support. The initial number of

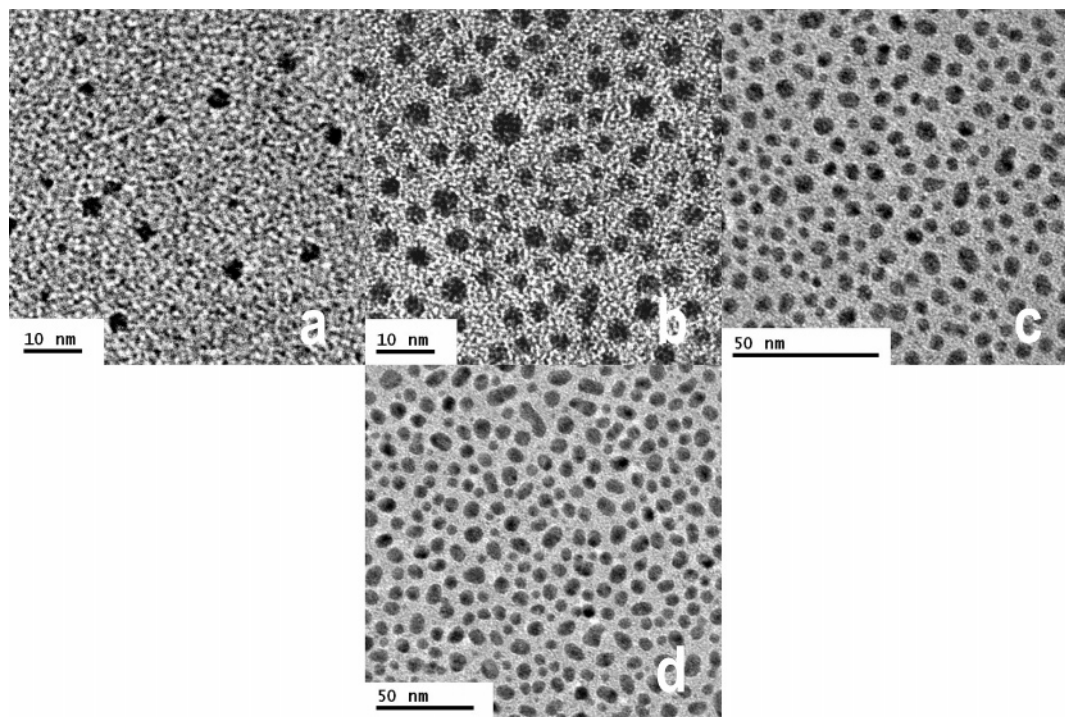


Figure 8. TEM micrographs of carbon (deposited by the carbon-coating system)-supported gold particles. The nominal thickness of gold was (a) 0.13, (b) 0.78, (c) 1.56, and (d) 2.33, and the deposition rate was $1.7 \times 10^{-3} \text{ nm s}^{-1}$.

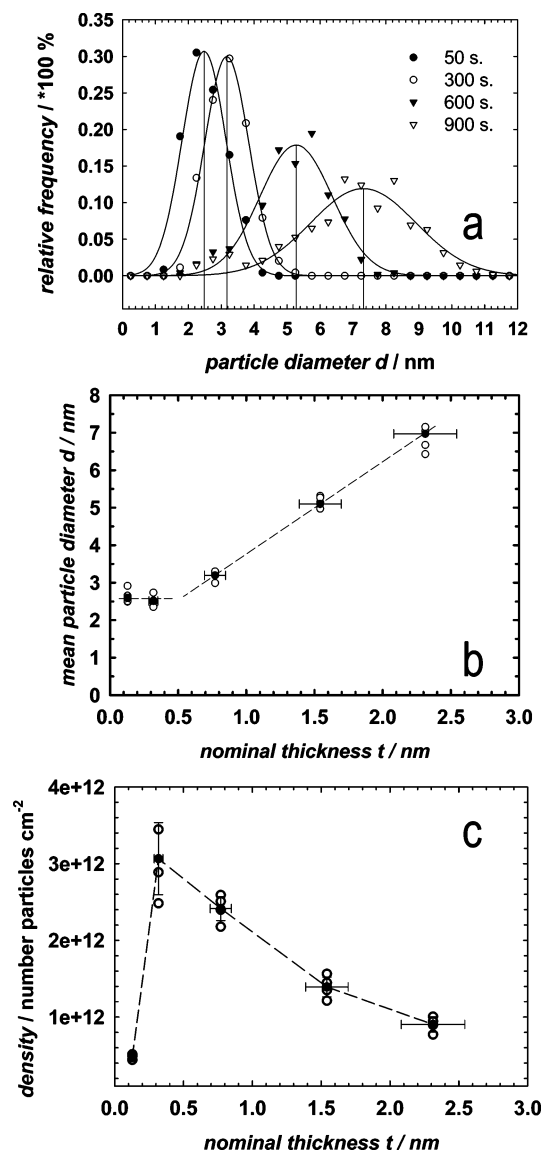


Figure 9. (a) Particle size distributions of gold particles grown on carbon (carbon coating system) obtained from TEM measurements. Gold deposition times are shown in the figure. The data were fitted to a normal Gaussian function. (b) The mean particle size of gold. (c) The number of particles per square centimeter of particles per square centimeter.

nucleation sites on carbon is considerably smaller than on titania during the initial Au deposition, resulting in larger particle sizes. As the number of nucleated particles grows at low nominal thickness, the average particle size is 2.5–3 nm. Particles coalesce at higher nominal thicknesses (at particles sizes where coalescence is observed on titania), and a concomitant reduction in number of particles per square centimeter is observed. At substrate temperatures of 325 K, we were not able to observe particles of Au on carbon below 2.5 nm.

Conclusion

A system designed for high-throughput physical vapor deposition of materials¹ has been applied to the synthesis of libraries of supported metal particles. Amorphous TiO_x supports have been synthesized with a controlled variation in stoichiometry in the range $x = 1.7$ – 1.9999 , as evidenced

by their range of conductivities. A range of Au nanoparticles have been synthesized as a function of position across titania substrates at a temperature of ~ 300 K. TEM measurements indicate that during nucleation, a mean particle size of 1.4 nm is observed, and increasing coverage leads to an increased number of such nuclei to a maximum density of $5.5 \times 10^{12} \text{ cm}^{-2}$. Particle sizes increase at higher Au coverages with a concomitant decrease in density. The small particles exhibit a binding energy shift in the Au(4f) core level of 0.3 eV from bulk gold, and the shift is 0.1 eV by the time particles grow to a mean size of 2.5 nm. Nucleation and growth of Au on carbon support is also observed, but the initial particle size is significantly larger at ~ 2.5 nm, and the maximum particle density ($3.1 \times 10^{12} \text{ cm}^{-2}$) is lower when compared to titania. The HT-PVD technique is a powerful method of producing supported metal samples of controlled particle size, and when combined with multiple source deposition¹ should allow similar control of supported alloy particles as a function of particle size and alloy composition. When combined with suitable screening methods,³⁴ the methodology provides a powerful route to the elucidation of particle size effects in catalysis on well-characterized model catalysts.

Acknowledgment. The authors acknowledge the General Motors Corporation for their financial support of this program and F.T. Wagner and H.A. Gasteiger for helpful discussions of the results. The authors also acknowledge the technical support of R. Greef with the ellipsometric measurements.

References and Notes

- Guerin, S.; Hayden, B. E. *J. Comb. Chem.* **2006**, *8*, 66.
- Guerin, S.; Hayden, B. E.; Lee, C. E.; Mormiche, C.; Owen, J. R.; Russell, A. E. *J. Comb. Chem.* **2004**, *6*, 149.
- Guerin, S.; Hayden, B. E.; Lee, C. E.; Mormiche, C.; Russell, A. E. *J. Phys. Chem. B* **2006**, in press.
- Kinoshita, K. *Carbon: Electrochemical and Physicochemical Properties*; Wiley: New York, 1988.
- Landsman, D.; Luczak, F. *Catalyst Studies and Coatings. In Handbook of Fuel Cells—Fundamentals, Technology and Applications*; Vielstich, W., Gasteiger, H. A., Lamm, A., Eds.; Wiley: Chichester, 2003; Vol. 4.
- Pletcher, D.; Walsh, F. C. *Industrial Electrochemistry*; Chapman and Hall: 1990.
- Haruta, M.; Date, M. *Appl. Catal. A* **2001**, *222*, 427.
- Haruta, M.; Tsubota, S.; Kobayashi, T.; Kageyama, H.; Genet, M. J.; Delmon, B. *J. Catal.* **1993**, *144*, 175.
- Date, M.; Okumura, M.; Tsubota, S.; Haruta, A. *Angew. Chem. Int. Ed.* **2004**, *43*, 2129.
- Cameron, D.; Holliday, R.; Thompson, D. *J. Power Sources* **2003**, *118*, 298.
- Valden, M.; Pak, S.; Lai, X.; Goodman, D. W. *Catal. Lett.* **1998**, *56*, 7.
- Valden, M.; Lai, X.; Goodman, D. W. *Science* **1998**, *281*, 1647.
- Yang, Z.; Wu, R.; Goodman, D. W. *Phys. Rev. B* **2000**, *61*, 14066.
- Cosandey, F.; Madey, T. E. *Surf. Rev. Lett.* **2001**, *8*, 73.
- Bocuzzi, F.; Chiorino, A.; Manzoli, M.; Lu, P.; Akita, T.; Ichikawa, S.; Haruta, M. *J. Catal.* **2001**, *202*, 256.
- Lopez, N.; Norskov, J. K. *Surf. Sci.* **2002**, *515*, 175.
- Lopez, N.; Janssens, T. V. W.; Clausen, B. S.; Xu, Y.; Mavrikakis, M.; Bligaard, T.; Norskov, J. K. *J. Catal.* **2004**, *223*, 232.
- Minato, T.; Susaki, T.; Shiraki, S.; Kato, H. S.; Kawai, M.; Aika, K.-i. *Surf. Sci.* **2004**, *556*–*568*, 1012.
- Chen, M. S.; Goodman, D. W. *Science* **2004**, *306*, 252.

- (20) Robertson, J. *Adv. Phys.* **1086**, 35, 317.
- (21) Hauge, P. S.; Dill, F. H. *Opt. Commun.* **1975**, 14, 431.
- (22) Diebold, U. *Surf. Sci. Rep.* **2003**, 48, 53.
- (23) Diebold, U. *Appl. Phys. A: Solids Surf.* **2003**, 76, 681.
- (24) Yagi, E.; Hasiguti, R. R.; Aono, M. *Phys. Rev. B: Condens. Matter Mater. Phys.* **1996**, 54, 7945.
- (25) Hayfield, P. C. S. *Development of a New Material- Monolithic Ti₄O₇ Ebonex Ceramic*; Royal Society of Chemistry: Letchworth, U.K., 2002.
- (26) Weast, R. C. *CRC Press* **1974**, 0, 0.
- (27) Guerin, S.; Hayden, B. E.; Pletcher, D.; Rendall, M. E.; Suchsland, J.-P.; Williams, L. *J. Comb. Chem.* **2006**, submitted.
- (28) Wahlstrom, E.; Lopez, N.; Schaub, R.; Thostrup, P.; Ronnau, A.; Africh, C.; Laegsgaard, E.; Norskov, J. K.; Besenbacher, F. *Phys. Rev. Lett.* **2003**, 90, .
- (29) Sykes, H.; Charles, E.; Williams, F. J.; Tikhov, M. S.; Lambert, R. M. *J. Phys. Chem B* **2002**, 106, 5390.
- (30) Zhang, L.; Persaud, R.; Madey, T. E. *Phys. Rev. B: Condens. Matter Mater. Phys.* **1997**, 56, 10549.
- (31) Zhang, L.; Cosandey, F.; Persaud, R.; Madey, T. E. *Surf. Sci.* **1999**, 439, 73.
- (32) Briggs, D.; Seah, M. *Practical Surface Analysis by Auger and X-ray Photoelectron Spectroscopy*; John Wiley & Sons Ltd.: Chichester, 1983.
- (33) Howard, A.; Clark, D. N. S.; Mitchell, C. E. J.; Egdell, R. G.; Dhanak, V. R. *Surf. Sci.* **2002**, 518, 210.
- (34) Guerin, S.; Hayden, B. E.; Pletcher, D.; Rendall, M. E.; Suchsland, J.-P. *J. Comb. Chem.* **2006**, in press.

CC060040K